Facile Heterogeneously Catalyzed Nitrogen Fixation by MXenes

José D. Gouveia,[†] Ángel Morales-García,[‡] Francesc Viñes,[‡] José R. B. Gomes[*,†] Francesc Illas,[*‡]

[†]*CICECO – Aveiro Institute of Materials, Department of Chemistry, University of Aveiro, Campus Universitário de Santiago, Aveiro, Portugal*

[‡]*Departament de Ciència de Materials i Química Física & Institut de Química Teòrica i Computacional (IQTCUB), Universitat de Barcelona, c/ Martí i Franquès 1-11, 08028 Barcelona, Spain*

Abstract: The rate-limiting step for ammonia (NH_3) production *via* the Haber-Bosch process is known to be the dissociation of molecular nitrogen (N_2), which requires quite harsh working conditions, even when using appropriate heterogeneous catalysts. Here, motivated by the demonstrated enhanced chemical activity of MXenes —a new class of two-dimensional inorganic materials— towards the adsorption of quite stable molecules such as CO_2 and H_2O, we use density functional theory including dispersion to investigate the suitability of such MXene materials to catalyze the N_2 dissociation. Results show that MXenes exothermically adsorb N_2, with rather large adsorption energies ranging from -1.11 to -3.45 eV and elongation of the N_2 bond length by ~20%, greatly facilitating its dissociation with energy barriers below 1 eV, reaching 0.28 eV in the most favorable studied case of W_2N. Microkinetic simulations indicate that the first hydrogenation of adsorbed atomic nitrogen is feasible at low pressures and moderate temperatures, and that the production of NH_3 may occur above 800 K on most studied MXenes, in particular in W_2N. These results reinforce the promising capabilities of MXenes to dissociate nitrogen and suggest combining them co-catalytically with Ru nanoparticles to further improve the efficiency of ammonia synthesis.

Keywords: 2D Materials; Adsorption; Ammonia Synthesis; Clean MXenes; Density Functional Theory; Metal Carbides and Nitrides; Microkinetic Modeling.

Introduction

Ammonia (NH_3) is the essential precursor in the synthesis of many N-containing compounds,[1,2] several of them having a high impact in our daily life, from sterilizing and cleaning products, to fertilizers and medicines.[3] Moreover, NH_3 emerges as an alternative energy carrier to reduce the fossil fuel consumption due to its large hydrogen capacity (17.6 wt%) and its energy density of 22.5 MJ/kg, comparable to that of fossil fuels such as low-ranked coals (around 20 MJ/kg).[4] The growing NH_3 demand has motivated a great interest in the artificial N_2 fixation.[5] However, the high N_2 stability, with a triple covalent bond dissociation energy of almost 10 eV, makes its chemical capture and activation a real challenge. In fact, industrial NH_3 synthesis *via* the Haber-Bosch (HB) process requires appropriate catalysts working at high temperatures (400-500 ºC) along with high pressures (100-300 bar) due to thermodynamic constraints.[6]

In particular, fused iron catalysts are well consolidated catalysts for HB synthesis.[7] The origin of the catalytic activity of Fe surfaces towards N_2 has been disclosed in several landmark surface science studies.[8-11] For instance, an experimentally-measured kinetic energy barrier of ~0.80 eV for N_2 dissociation on Fe(111) has been reported at near-operational HB conditions.[12] More recently, small iron Fe_3 supported on the θ-Al_2O_3(010) surface have been also proposed as feasible heterogeneous catalyst for ammonia synthesis.[13] Other suitable catalysts such as Ru nanoparticles (NPs),[14] graphene-based substrates ($GraN_4$-Cr),[15] and dicoordinate borylenes[16] have been recently explored, all displaying good catalytic activity for N_2 dissociation. For instance, energy barriers for N_2 dissociation in the 0.4–1.9 eV interval have been predicted for the reaction on Ru nanoparticles, depending on whether terrace or step sites are considered as catalytic active sites. Similar dissociation barriers are found on well-defined V(110) surfaces.[17] Despite the fact that active sites at operating conditions could not necessarily coincide with those exhibiting the lowest energy barriers,[14,17] a small energy barrier for N_2 dissociation is still considered as a requisite for an efficient conversion. Consequently, research endeavors are aimed at finding improved catalysts that can potentially operate HB synthesis at milder conditions.[18]

Recently, a fast-growing family of two-dimensional (2D) inorganic materials, usually referred to as MXenes, has been isolated by HF selective etching from precursor MAX phases.[19] The resulting 2D flake materials have been fully characterized as made up of close-packed layers of transition metals (M = Ti, Zr, Hf, V, Nb, Ta, Cr, Mo, or W) intercalated by layers of carbon or nitrogen (X = C or N), with the general formula $M_{n+1}X_nT_x$ (n = 1–3), where T_x represents the surface terminations bonded to the outer M layers.[20] MXenes may display different T_x terminations depending on the synthesis conditions, with O, OH, F, and H being the most common.[21] More recently, HF-free syntheses have been reported where MXenes are terminated by H and OH only.[22,23] In addition, post-synthesis heating treatments have been shown to successfully defunctionalize MXene surfaces.[24,25] When devoid of T_x, MXenes are naturally quite reactive and are known to strongly adsorb molecules, facilitating their posterior conversion. The use of MXenes in catalysis has been reviewed very recently.[26] Other, recent examples include CO_2 and H_2O adsorption and

dissociation.[27-29] In addition, the possibility to use conducting MXenes as electrodes in electrocatalysis has also been considered. In particular, Seh *et al.*[30] explored the performance of Mo_2CT_x and Ti_2CT_x as electrocatalysts in the hydrogen evolution reaction (HER), whereas Yi *et al.*[31] theoretically studied the performance of a Ti_2C monolayer as a cathode substrate to improve the performance of the Li–N_2 battery. The latter authors found a very strong interaction between N_2 and the bare Ti_2C and, interestingly, the presence of Li atoms seemed to facilitate the N_2 dissociation. In another computational keynote work, Azofra *et al.*[32] investigated the mechanism of NH_3 electrocatalytic synthesis from N_2 using a family of M_3C_2 MXenes as catalysts. These two previous studies on the N_2 electrochemical reduction considered a mechanism involving a series of proton-electron transfers,[33] resulting in the successive hydrogenation of one or both N atoms of N_2, thus, concomitantly weakening the N≡N bond and eventually leading to the NH_3 formation.[34-38] However, it is worth pointing out that the literature of N_2 reduction *via* heterogeneous catalysis on MXenes is scarce, despite the demonstrated stability of these surfaces in inert, oxidizing, and reducing environments (*e.g.* V_2CT_x),[39] and thermal stability (800 ºC at least), which open the possibility of using MXenes at *operando* conditions of the HB process.[24] In the case of the $Ti_3C_2T_x$ MXene, thermal and mechanical stabilities were reported up to a temperature of 900 ºC and a pressure of 26.7 GPa.[40,41] Recent computational studies also provide compelling evidence that bare MXene materials are mechanically and dynamically stable.[42] All these findings strongly suggest that MXenes could display an efficient activity towards heterogeneous catalytic N_2 dissociation and, eventually, towards NH_3 synthesis in the HB process. Motivated and inspired by this, the present work explores the chemical activity of 18 MXenes from groups IV-VI —nine carbide and nine nitride MXenes— towards N_2 adsorption and subsequent direct dissociation by means of density functional theory (DFT) methods and microkinetic modeling. The obtained results confirm the hypothesis that these new materials can dissociate N_2 at rather mild conditions, which may have implications in the N_2 utilization in general, and on the ammonia synthesis in particular.

MXene Models and Computational Details

To understand the nitrogen fixation by MXenes, the N_2 dissociation mechanism was firstly investigated, using first-principles calculations as implemented in the Vienna *ab initio* simulation package (VASP).[43] Then, the potential energy diagram for NH_3 synthesis from N_2 and H_2 on selected surfaces was thoroughly investigated. The MXenes basal (0001) surfaces are modeled by a periodic hexagonal *p*(3×3) supercell containing 27 atoms (Figure 1), with lattice parameters as displayed in Table S1 of the Supporting Information (SI). The valence electron densities have been expanded in a plane wave basis set with a cutoff for the kinetic energy of 415 eV, whereas the effects of the core electrons on the valence electron densities were taken into account by means of the projector-augmented wave (PAW) method.[44] The Brillouin zone was sampled using a Monkhorst-Pack 5×5×1 grid of **k**-points.[45] The calculations were carried out within the generalized gradient approximation (GGA), using the Perdew, Burke, and Ernzerhof (PBE) exchange-correlation functional[46], including dispersion interactions through the Grimme D3 method.[47] The convergence criteria for the self-consistent energies and forces for relaxed structures were set to 10^{-6} eV and

0.01 eV·Å^{-1}, respectively. Spin polarization was found to be necessary to properly describe the Ti_2C, Zr_2C, and Cr_2C MXenes. Further details regarding the definition of adsorption energy and related quantities as well as Gibbs free energies calculation are reported in the SI.

Results and discussion

The interactions of atomic and molecular nitrogen with the above-mentioned MXene surfaces have been investigated by sampling four relevant high-symmetry sites, see Figure 1. On most MXenes the N atom adsorbs preferably on the H_M site, yet in the case of W_2C and d^4 nitrides the H_X site is energetically favorable. The calculated N adsorption energies relative to $^1/_2 \cdot E_{N_2}$ for carbide and nitride MXenes are all negative indicating exothermic adsorptions —see Table S2 of the SI for further details. In general, the atomic N adsorption becomes weaker as one moves from d^2 to d^4 MXenes. The N_2 molecule adsorbs in a similar way on all MXenes, with one of the N atoms lying above an H_M site and the other above a nearby H_X site —B site for Mo_2C, W_2C, Nb_2N, and Ta_2N— with results summarized in Table 1 and Figure 2. For the H_M-H_X adsorption configurations, the molecule adsorbs approximately parallel to the plane of the surface, with a titling angle of ~15º. In both configurations, the N atom closest to the surface is placed ~1 Å above the metal atoms layer and the N-N distance is ~1.35 Å, *i.e.* about 20% longer than the corresponding gas phase value of 1.11 Å. Analogously to N adsorption, N_2 adsorption is stronger on d^2 MXenes and becomes weaker as we move to d^3 and d^4 metals.

The large N_2 adsorption energy and the noticeable bond length elongation are already indicative of N_2 activation, and so, forecast an easy N_2 dissociation. However, a firm statement requires locating the N_2 dissociation transition state (TS) along different breaking pathways on the studied MXene surfaces. The TSs have been determined and characterized as indicated in the SI. All of them can be described as early states, since the corresponding structure closely resembles the initial configuration just with the N atoms slightly farther from each other, ~1.8 Å. Taking Zr_2C as an example, the most favorable adsorption site of N_2 is H_M-H_C, whereas the N atoms adsorb on H_M sites, see Figure 2. The associated TS structure keeps one N at H_M while moving the other farther away, so that, after the molecular dissociation, both N adatoms sit at H_M sites. However, in the case of Nb_2C, Ta_2N, and W_2N, the configuration after dissociation is such that one of the N adatoms remains on its most stable adsorption site, while the second one sits on the nearest hollow site at a distance of around 2.5 times the calculated N_2 bond length. In this situation, there is a strong lingering lateral interaction between the two N adatoms that is released by moving the second N adatom to its most favored adsorption site. Table 1 compiles the related energies and shows that the calculated energy barriers, E_b, range from 0.28 to 1.1 eV, tending to decrease along the group or period of the metal. This implies that E_b is often smaller than the N_2 adsorption energy, a feature not easily fulfilled by standard catalysts and the reason why high pressures are needed in the HB process. All dissociation steps are found to be exothermic, with reaction energies, E_{reac}, as large as -3.19 eV on W_2N, and exothermicity increasing as the group or period of the MXene increases. Hence, the most exothermic dissociation occurs on the MXene with the

lowest E_b, suggesting that the overall process may follow a Brønsted-Evans-Polanyi (BEP) relationship.[48-50] Indeed, the plot in Figure 3 of E_b *vs.* E_{reac} shows that BEP holds and leads to a faster way to predict results for other possible MXenes.

To go beyond the previous thermodynamic and kinetic analyses and to account for real *operando* conditions, we consider the variation of the Gibbs free energy of adsorption of the reacting systems at 1 bar and 300 K —see details in the SI. For all the studied MXenes, trends in Gibbs free energy of adsorption of N and N_2 are similar to those reported for E_{ads} although weaker by 0.25 and 0.50 eV, respectively. The reaction energy values are practically unaffected by temperature and pressure, with differences lower than 0.01 eV with respect to the values listed in Table 1, while E_b values are reduced by *circa* 0.06 eV. From this set of results, one can conclude that increasing the temperature is, if any, beneficial for the dissociation of N_2 on MXenes, as it both lowers the E_b values and contributes towards replacing the MXene surface termination by N_2. Furthermore, the obtained values do not seem to be assignable solely to the explored M:X 2:1 stoichiometry, as test simulations for N_2 dissociation on the experimentally isolated Ti_4N_3, Nb_4C_3, and Ta_4C_3, all 4:3 stoichiometric MXenes,[51,52] yield nearly identical results to those obtained for the M_2X stoichiometry, with E_{ads} and E_b values differing by up to 0.05 eV at most. These findings strongly support that conclusions taken from the present calculations are likely to apply to thicker MXenes as well, in line with the already reported very small variation of the CO_2 capture capabilities of MXenes of different thickness.[53]

To further assess the catalytic capability of MXene for nitrogen fixation, we compare the present results with available data in the literature. To this end we rely on E_b values for N_2 dissociation although a comparison of present and previously reported N_2 adsorption energies on MXenes is provided in the SI. In the case of Ti_2C, the present value for E_b of 0.98 eV compares well with the 1.17 eV value reported by Yi *et al.*[31] Note, however, that the latter has been acquired in the different context of the electrocatalytic HER. In any case, to find that these two values are only slightly larger than the experimentally measured barrier of 0.80 eV for N_2 dissociation on Fe (111) at conditions close to the ones required for the HB process[12] is really remarkable. Encouragingly, lower E_b values are predicted for other MXenes, see Table 1, where W_2N MXene (0001) surface features the lowest value of 0.28 eV. It is worth to point that this activation barrier is similar to that reported for the step regions of Ru surfaces[54] and on a cesium-promoted ruthenium particle supported on MgO[55] that show 0.40 and 0.34 eV, respectively (Tables S3 and S5). Nevertheless, other MXenes exhibit quite low E_b values close to 1.0 eV. In general, carbide and nitride MXenes emerge as potentially suitable materials for N_2 dissociative adsorption with a reactivity comparable or even superior to other reported transition metal surfaces or NPs.[12,14,17] Therefore, MXenes appear as potential catalysts candidates for N_2 fixation; *i.e.* in the NH_3 synthesis. However, the latter requires considering the successive N adatom hydrogenation steps as well. These have been studied in detail for Nb_2C, Mo_2N, and W_2N, chosen because of their low N_2 dissociation energy barriers. The total and Gibbs free energy profiles at standard conditions, plotted in Figure 4, reveal that, for such a catalyzed process, the rate-limiting step would be these

hydrogenation steps instead of the N_2 dissociation one. Actually, for the three systems with smallest N_2 dissociation barriers, the energy barriers for these hydrogenation steps are somewhat higher than those reported, for instance, on a model Ru (001) surface,[54] yet surmountable at working conditions, especially for W_2N. At this point, it is worth considering whether PBE results provide an accurate enough comparison to experiment.[56] From Figure 4, it is clear that, as expected, PBE poorly describes the gas phase thermochemistry of this reaction (see gray lines in Figure 4). Nevertheless, there is compelling evidence that this DFT approach performs satisfactorily for surface reactions,[14] where the electron density is less localized. This is further supported by the good agreement between experimental turnover frequencies and predictions from kinetic Monte Carlo and microkinetic simulations using DFT derived rates.[57,58]

To further assess the capability of MXenes for ammonia synthesis, microkinetic simulations were carried out to obtain insights into the production of NH_3 on W_2N by using the MKMCXX program[59,60] — further details of the microkinetic simulations are given in the SI. Note that the choice of the W_2N MXene is justified as this material exhibits the lowest energy barriers for N_2 dissociation and subsequent hydrogenation steps leading to the formation of ammonia, see Table S3. The simulations were carried out taking a gas phase mixture with a N_2:H_2 molar ratio of 1:3 at 1 bar. Two limiting cases were studied separately; assuming that after N_2 dissociation the two N* species are located at the nearby surface sites, or that instead they immediately migrate to outlying regions, see Figure 5. In the first scenario, displayed in Figures 5a and 5b, the formation of NH* is predicted to take place at 1 bar and below 600 K. However, the backward reactions towards the N* and H* species are favored by higher temperatures. This simulation confirms that the formation of NH_3 could be affordable (Figure 5b) reaching the maximum of production at 1075 K, where the apparent activation energy is zero (Figure S2). The reaction orders of N_2 and H_2 as a function of temperature are depicted in Figure S3. From this figure, it can be seen that the reaction orders of the reactants increase with temperature, they are related with the decreasing of the coverage, in consistency with Figure 5a. The degree of rate control (DRC) shown in Figure S4, concludes that the NH_2+H recombination on the W_2N MXene (0001) surface is the rate-limiting step. Finally, the rates of the reaction following eight elementary reaction steps are depicted in Figure S5. In the second situation, the W_2N catalyst is poisoned by the N^* species (Figure 5c) and, consequently, the formation of NH_3 does not take place. Interestingly, the differences between these two situations may be found in the backward reaction, which corresponds to the recombination of the N* species into N_2, see Table S5. These activation barriers are 1.12 and 3.46 eV for the nearby and outlying situation, respectively. In conclusion, a large backward energy barrier indicates that the W_2N MXene dissociates the nitrogen molecule poisoning the surface and cutting the reaction off. For the most interesting scenario, *i.e.* N* species adsorbed at nearby surface sites, results from microkinetic simulations in Figures S6-S8 obtained for a gas phase mixture with N_2:H_2 molar ratio of 1:3 but at a higher pressure, *viz.* 200 bar, show that it is not only possible to form significant amounts of NH* but that it is possible to reach NH_2* at temperatures below 600 K.

The present computational study strongly suggests that MXenes may constitute appropriate materials for dissociating the N_2 molecule even at standard pressure, reporting better forward activation barriers for the dissociation of N_2 molecule than Ru nanoparticles, see Table S5. Finally, although the hydrogenation of easily formed N adatoms on MXenes may be more difficult, other strategies can be envisaged to overcome this possible hurdle, *e.g.* using MXenes as a support material for Ru NPs[61] in a tandem, bifunctional catalyst, with the MXene substrate adsorbing and dissociating N_2, whereas the Ru active centers would be better suited in hydrogenating the formed N adatoms towards NH_3, thus ideally permitting the Haber-Bosch NH_3 synthesis at milder conditions.

Conclusions

To summarize, MXenes are introduced here as potential catalysts to adsorb and exothermically dissociate N_2 at mild conditions, with energy barriers ranging from 0.28 to 1.10 eV, which are comparable to, or even lower than, those corresponding to models of transition metal-based industrial catalysts. Even though the present conclusions hold for MXenes with M:X 2:1 ratio, additional simulations on MXenes with 4:3 ratio revealed negligible material thickness effect. Moreover, the fact that the N adatom hydrogenation steps are somewhat more costly than the same steps on commercial transition metal-based catalysts suggests synergistically using MXenes as supports of metal nanoparticles used in the Haber-Bosch process leading to bifunctional catalysts with better activities at a lower cost. The remarkable chemistry of MXenes towards N_2 suggest that they could be used in the Haber-Bosch ammonia synthesis. Nevertheless, additional work from both modelling and experimental points of view are needed to further confirm this hypothetical and, at the same time, appealing catalytic activity.

Table 1 N_2 adsorption sites, adsorption energies, E_{ads}, dissociation energy barriers, E_b, and dissociation reaction energies, E_{reac}, on the studied MXene (0001) surfaces. The N_2 adsorption site is specified by the surface sites occupied by the two nitrogen atoms, see Figure 1. All values are given in eV and include the zero point energy (ZPE) contribution.

		M_2C				**M_2N**			
	M	**Site**	E_{ads}	E_b	E_{reac}	**Site**	E_{ads}	E_b	E_{reac}
d^2	**Ti**	H_M-H_C	-3.26	0.98	-1.55	H_M-H_N	-3.45	0.93	-2.00
	Zr	H_M-H_C	-2.84	1.10	-1.60	H_M-H_N	-3.08	0.91	-2.25
	Hf	H_M-H_C	-3.14	0.96	-2.02	H_M-H_N	-3.30	0.75	-2.61
d^3	**V**	H_M-H_C	-2.99	0.80	-1.77	H_M-H_N	-2.10	0.78	-2.20
	Nb	H_M-H_C	-2.41	0.75	-2.18	H_M-B	-1.76	0.60	-2.70
	Ta	H_M-H_C	-2.35	0.53	-2.72	H_M-B	-2.12	0.48	-3.06
d^4	**Cr**	H_M-H_C	-2.12	0.85	-1.90	H_M-H_N	-1.66	0.61	-1.85
	Mo	H_M-B	-1.59	0.93	-2.35	H_M-H_N	-1.55	0.45	-2.76
	W	H_M-B	-1.11	0.37	-2.48	H_M-H_N	-1.34	0.28	-3.19

Figure 1. Top view of the *p*(3×3) supercell employed to model the MXene (0001) surfaces. The transition metal atoms are shown as grey spheres, while X atoms are shown as green spheres. The dashed rhombus represents the boundaries of the employed supercell. The labels refer to the four relevant high-symmetry sites on the surface: bridge (B), top (T), hollow metal (H_M), and hollow carbon/nitrogen (H_X) —in practice, H_C or H_N.

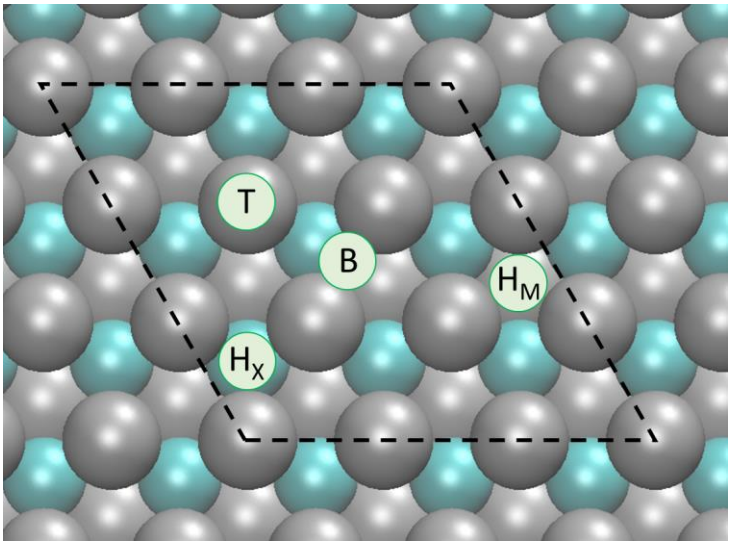

Figure 2. Initial state (IS - left), transition state (TS - middle), and final state (FS – right) configurations of N_2 dissociation on the Zr_2C MXene (0001) surface, as seen from the side (top) and top (bottom) views. Color code as in Figure 1, N atoms are shown as dark blue spheres. Note that this particular case is representative for most carbide and nitride MXene (0001) surfaces investigated, while on Nb_2C, Mo_2N, Ta_2N, and W_2N the two N adatoms remain on their original H_M and H_X sites after dissociation, but about twice as far from each other as in the TS.

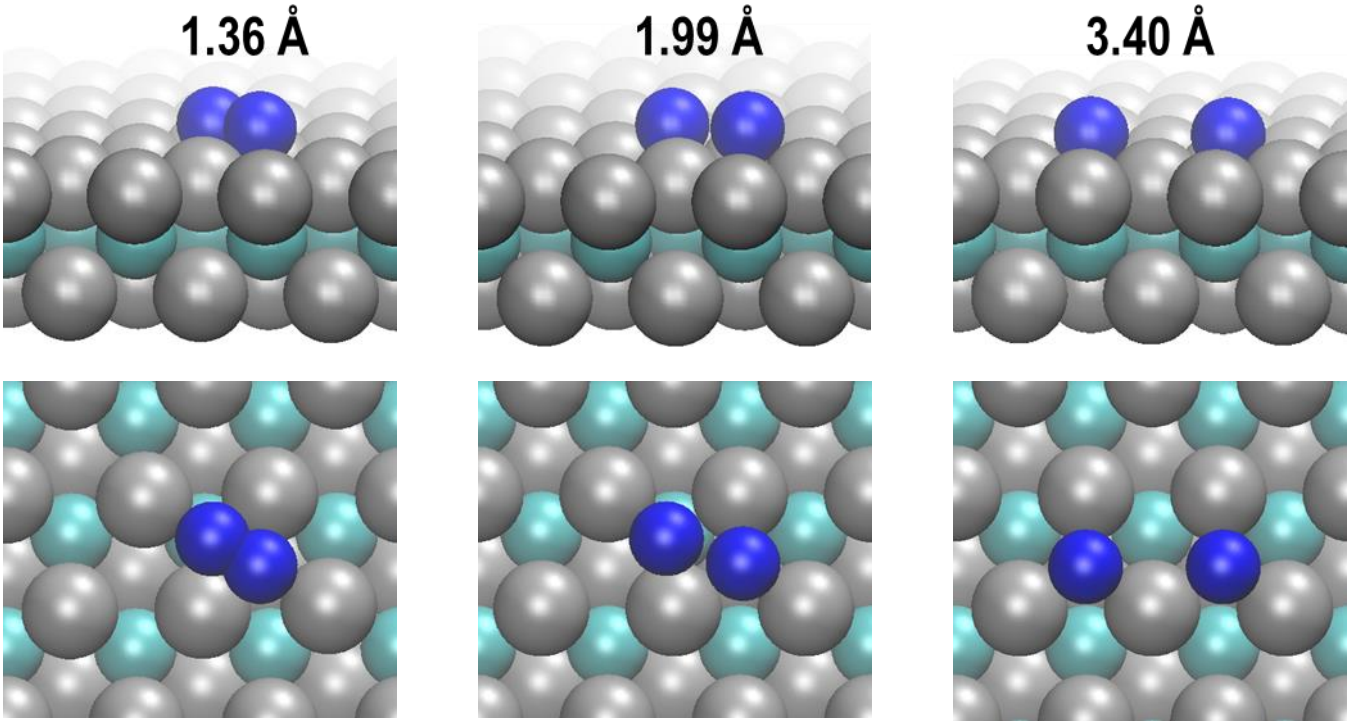

Figure 3. Plot of the BEP relationship for N_2 dissociation reaction energy barrier, E_b, and the dissociation energy, E_{reac}, on the MXene surfaces investigated; the black line defines the linear regression, with equation $E_b = 0.387 \cdot E_{reac} + 1.611$, and correlation coefficient R = 0.79. Blue and red dots correspond to carbide and nitride MXenes, respectively.

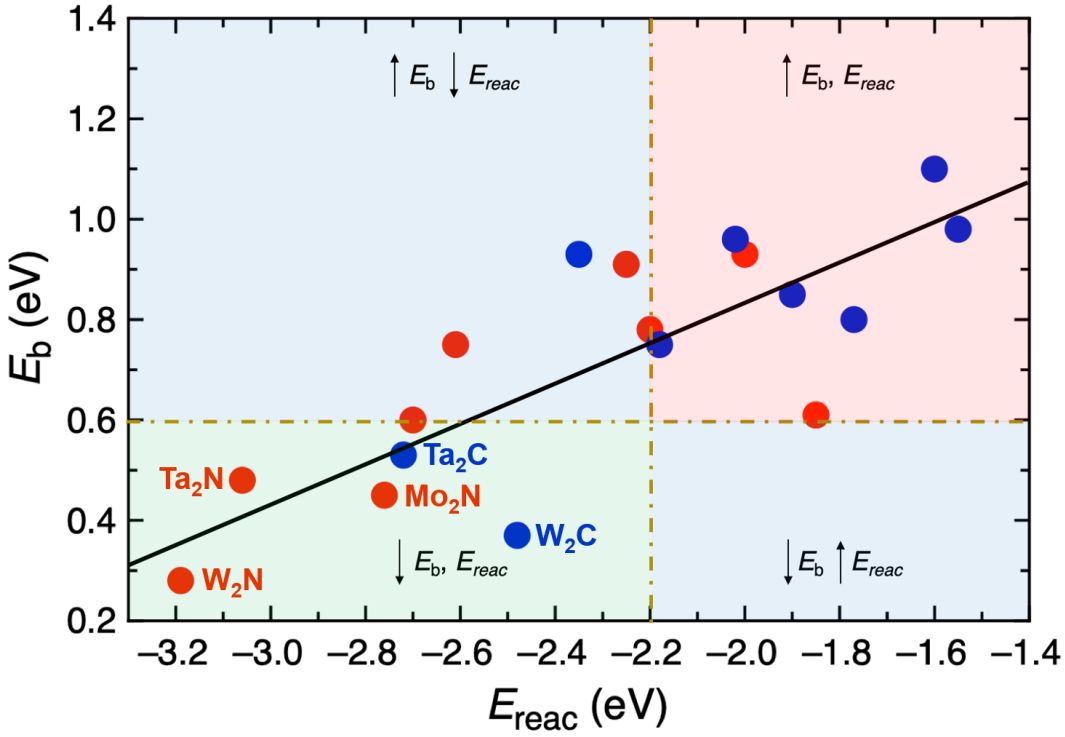

Figure 4. Total (top) and Gibbs (down) free energy reaction profiles of ammonia synthesis on Nb_2C (blue), Mo_2N (red), and W_2N (black) MXene (0001) surfaces. Gibbs energy profiles are obtained assuming a temperature of 300 K and N_2 and H_2 partial pressures of 1 bar. The energy barriers are collected in Table S3. Gray lines correspond to accurate thermochemistry description of this reaction in the gas phase, considering the golden standard coupled cluster with single, doubles, and perturbative triples —CCSD(T)— method (top), and the experimental reaction Gibbs energy at a working temperature of 300 K and a pressure of 1 bar for H_2 and N_2 gases (down). The CCSD(T)/cc-pVTZ calculations were taken from the Computational Chemistry Comparison and Benchmark Database (https://cccbdb.nist.gov/).

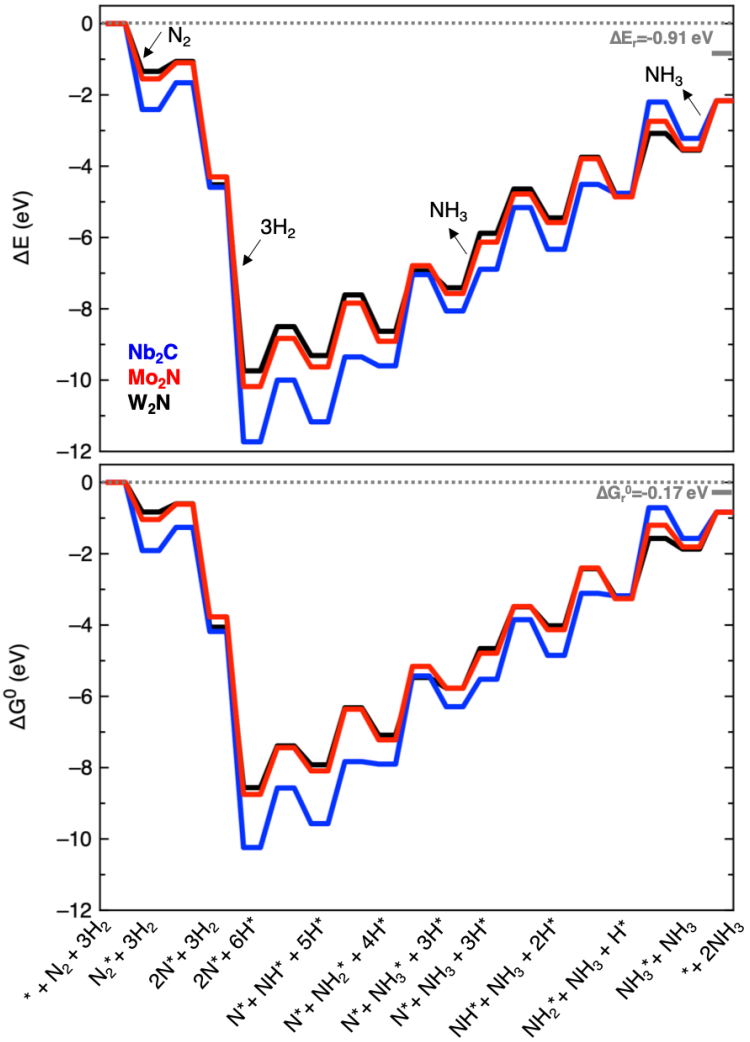

Figure 5. Results from microkinetic simulations performed on the W_2N MXene (0001). The gas phase contains a mixture of N_2 and H_2 in a 1:3 molar ratio at a total pressure of 1 bar. Two different scenarios are analyzed: (a) and (b) correspond to a situation where the N* species are close to each other (high-coverage), whereas in (c) and (d) the N* species are far from each other (low-coverage). The coverage of the most abundant species for the N_2 fixation on MXene surface along with the ammonia production as a function of the temperature are figures a-c and b-d, respectively for each of the investigated scenarios. The gray bar indicates the temperature conditions at which the industrial HB process takes place.

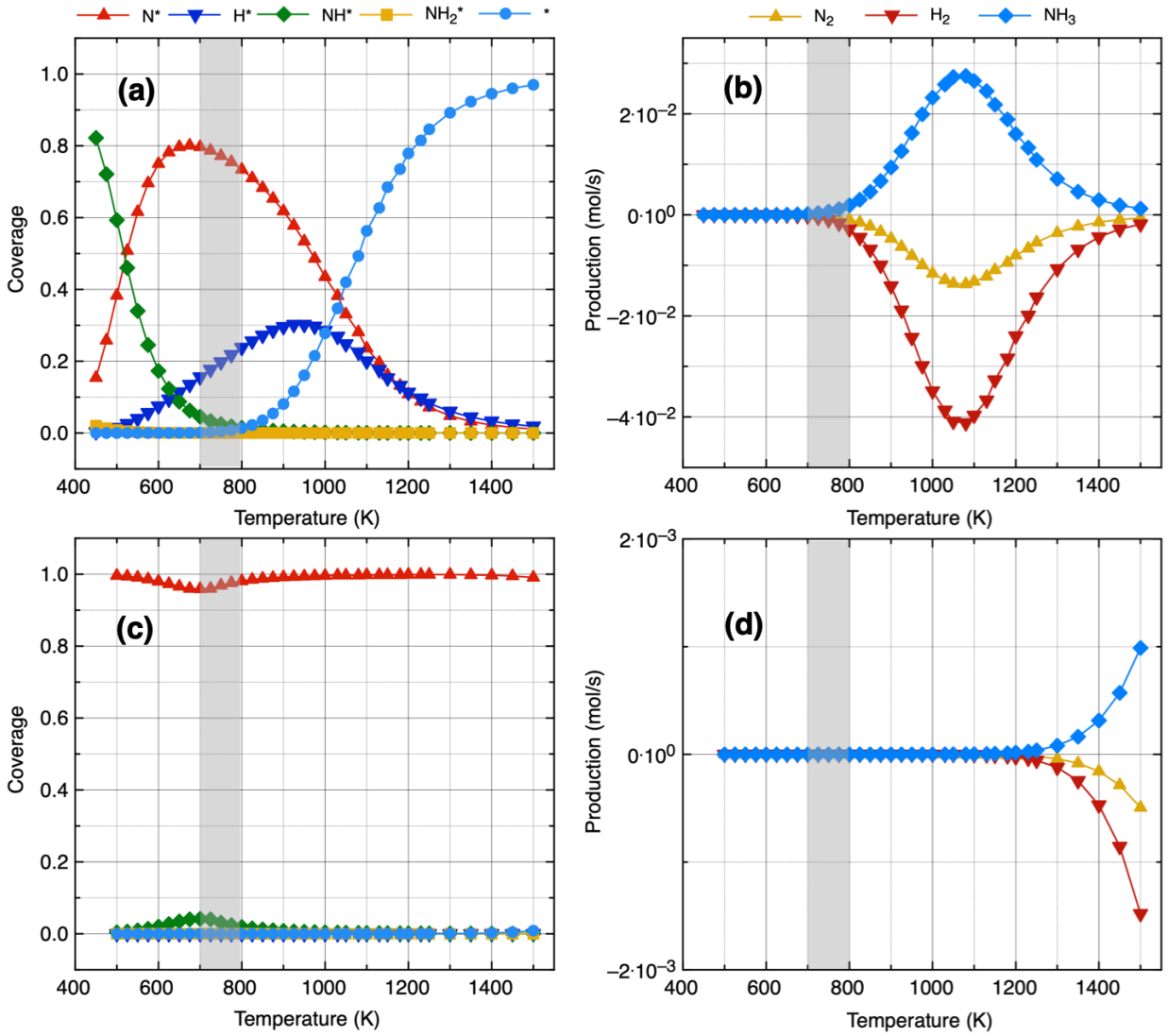

AUTHOR INFORMATION

Corresponding Authors

E-mails: jrgomes@ua.pt (ORCID: 0000-0001-5993-1385); francesc.illas@ub.edu (ORCID: 0000-0003-2104-6123)

Notes

The authors declare no competing financial interest.

ASSOCIATED CONTENT

The Supporting Information is available free of charge on the ACS Publications website at DOI:

Additional computational details and comparison to previous work. Tables S1 and S2 report the calculated lattice parameters and adsorption related properties. Tables S3 and S4 report the energy barriers of the total and Gibbs free energy reaction profiles of ammonia synthesis. Table S5 compiles a comparison of the forward and backward energy barriers corresponding to Ru NPs and W2N MXene (0001) surface. Figure S1 shows the configurations of transition states and ground state adsorption involved in the process of the triple hydrogenation of a nitrogen adatom. Figure S2 shows the apparent activation energy of the N2 fixation over W2N MXene (0001) surface resulted from the microkinetic simulations for the situation where the N* species are located in nearby regions. Additional references are also included.

Acknowledgements

The research carried out at the CICECO – University of Aveiro Institute of Materials was developed within the scope of projects UID/CTM/50011/2019 and POCI/01/0145/FEDER/007679, financed by the Portuguese *Fundação para a Ciência e a Tecnologia* (FCT/MCTES), and co-financed by the European Regional Development Fund (FEDER) under the PT2020 Partnership Agreement. The research carried out at the *Universitat de Barcelona* has been supported by the Spanish MICIUN/FEDER RTI2018-095460-B-I00 and *María de Maeztu* MDM-2017-0767 grants and, in part, by *Generalitat de Catalunya* 2017SGR13 and XRQTC grants. J.D.G. is also thankful to projects CENTRO-01-0145-FEDER-31002 (SILVIA) and HPC-EUROPA3 (INFRAIA-2016-1-730897) supported by the EC Research Innovation Action under the H2020 Programme. A. M.-G. thanks to Spanish MICIUN for his *Juan de la Cierva* (IJCI-2017-31979) postdoctoral grant, F. V. is thankful to *Ministerio de Economía y Competitividad* (MEC) for his *Ramón y Cajal* (RYC-2012-10129) research contract, and F. I. acknowledges additional support from the 2015 ICREA Academia Award for Excellence in University Research.

References

(1) Thomas, J. M., Thomas W. J. Principles and Practice of Heterogeneous Catalysis, 2nd Edition. Wiley-VCH, **2014**; 551-559.

(2) Wiberg, E.; Wiberg, N.; Holleman, A. F. Inorganic Chemistry. New York: San Diego: Academic Press, **2001**; 598-675.

(3) Lassaletta, L.; Billen, G.; Grizzetti, B.; Anglade, J.; Garnier, J. 50 Year Trends in Nitrogen Use Efficiency of World Cropping Systems: The Relationship Between Yield and Nitrogen Input to Cropland. *Environ. Res. Lett.* **2014**, *9*, 105011.

(4) Valera-Medina, A.; Xiao, H.; Owen-Jones, M.; David, W. I. F.; Bowen, P. J. Ammonia for Power. *Prog. Energ. Combust.* **2018**, *69*, 63-102.

(5) Li, H.; Mao, C.; Shang, H.; Yang, Z.; Ai, Z.; Zhang, L. New Opportunities for Efficient N_2 Fixation by Nanosheet Photocatalysts. *Nanoscale* **2018**, *10*, 15429-15435.

(6) Kandemir, T.; Schuster, M. E.; Senyshyn, A.; Behrens, M.; Schlögl, R. The Haber-Bosch Process Revisited: On the Real Structure and Stability of "Ammonia Iron" under Working Conditions. *Angew. Chem. Int. Ed.* **2013**, *52*, 12723-12726.

(7) H. Liu. Ammonia Synthesis Catalysts. World Scientific / Chemical Industry Press, China, **2013**; 185-309.

(8) Bozso, F.; Ertl, G.; Grunze, M.; Weiss M. Interaction of Nitrogen with Iron Surfaces: I. Fe(100) and Fe(111). *J. Catal.* **1977**, *49*, 18-41.

(9) Imbihl, R.; Behm, R. J.; Ertl, G.; Moritz, W. The Structure of Atomic Nitrogen Adsorbed on Fe(100). *Surf. Sci.* **1982**, *123*, 129-140.

(10) Ertl, G.; Lee, S. B.; Weiss, M. Kinetics of Nitrogen Adsorption on Fe(111). *Surf. Sci.* **1982**, *114*, 515-526.

(11) Ertl, G. Primary Steps in Catalytic Synthesis of Ammonia. *J. Vac. Sci. & Technol. A* **1983**, *1*, 1247-1253.

(12) Spencer, N. D.; Schoonmaker, R. C.; Somorjai, G. A. Iron Single Crystals as Ammonia Synthesis Catalysts: Effect of Surface Structure on Catalyst Activity. *J. Catal.* **1982**, *74*, 129-135.

(13) Liu, J.-C.; Ma, X.-L.; Li, Y.; Wang, Y.-G.; Xiao, H.; Li, J. Heterogeneous Fe_3 Single-Cluster Catalysts for Ammonia Synthesis via an Associative Mechanism. *Nat. Comm.* **2018**, *9*, 1610.

(14) Honkala, K.; Hellman, A.; Remediakis, I. N.; Logadottir, A.; Carlsson, A.; Dahl, S.; Christensen, C. H.; Nørskov, J. K. Ammonia Synthesis from First-Principles Calculations. *Science* **2005**, *307*, 555-558.

(15) Riyaz, M.; Goel, N. Single-Atom Catalysis Using Chromium Embedded in Divacant Graphene for Conversion of Dinitrogen to Ammonia. *ChemPhysChem* **2019**, *20*, 1954-1959.

(16) Légaré, M.-A.; Bélanger-Chabot, G.; Dewhurst, R. D.; Welz, E.; Krummenacher, I.; Engels, B.; Braunschweig, H. Nitrogen Fixation and Reduction at Boron. *Science* **2018**, *359*, 896-900.

(17) Rochana, P.; Lee, K.; Wilcox, J. Nitrogen Adsorption, Dissociation, and Subsurface Diffusion on the Vanadium (110) Surface: A DFT Study for the Nitrogen-Selective Catalytic Membrane Application. *J. Phys. Chem. C* **2014**, *118*, 4238-4249.

(18) Vojvodic, A.; Medford, A. J.; Studt, F.; Abild-Pedersen, F.; Khan, T. S.; Bligaard, T.; Nørskov, J. K. Exploring the Limits: A Low-Pressure, Low-Temperature Haber-Bosch Process. *Chem. Phys. Lett.* **2014**, *598*, 1018-112.

(19) Naguib, M.; Kurtoglu, M.; Presser, V.; Lu, J.; Niu, J.; Heon, M.; Hultman, L.; Gogotsi, Y.; Barsoum, M. W. Two-Dimensional Nanocrystals Produced by Exfoliation of Ti_3AlC_2. *Adv. Mater* **2011**, *23*, 4248–4253.

(20) Anasori, B.; Lukatskaya, M. R.; Gogotsi, Y. 2D Metal Carbides and Nitrides (MXenes) for Energy Storage. *Nat. Rev. Mater.* **2017**, *2*, 16098.

(21) Gogotsi, Y.; Anasori, B. The Rise of MXenes. *ACS Nano* **2019**, *13*, 8491-8494.

(22) Li, T.; Yao, L.; Liu, Q.; Gu, J.; Luo, R.; Li, J.; Yan, X.; Wang, W.; Liu, P.; Chen, B.; Zhang, W.; Abbas, W.; Naz, R.; Zhang, D. Fluorine-Free Synthesis of High-Purity $Ti_3C_2T_x$ (T = OH, O) *via* Alkali Treatment. *Angew. Chem. Intl. Ed.* **2018**, *57*, 6115-6119.

(23) Yu, X.; Cai, X.; Cui, H.; Lee, S.-W.; Yu, X.-F.; Liu, B. Fluorine-Free Preparation of Titanium Carbide MXene Quantum Dots with High Near-Infrared Photothermal Performance for Cancer Therapy. *Nanoscale* **2017**, *9*, 17859-17864.

(24) Persson, I.; Halim, J.; Lind, H.; Hansen, T. W.; Wagner, J. B.; Näslund, L.-A.; Darakchieva, V.; Palisaitis, J.; Rosen, J.; Persson, P. O. A. 2D Transition Metal Carbides (MXenes) for Carbon Capture. *Adv. Mater.* **2019**, *31*, 1805472.

(25) Deeva, E. B.; Kurlov, A.; Abdala, P. M.; Lebedev, D.; Kim, S. M.; Gordon, C. P.; Tsoukalou, A.; Fedorov, A.; Müller, C. R. In Situ XANES/XRD Study of the Structural Stability of Two-Dimensional Molybdenum Carbide Mo_2CT_x: Implications for the Catalytic Activity in the Water–Gas Shift Reaction. *Chem. Mater.* **2019**, *31*, 4505-4513.

(26) Li, Z.; Wu, Y. 2D Early Transition Metal Carbides (MXenes) for Catalysis. *Small* **2019**, *15*, 1804736.

(27) Morales-García, Á.; Fernández- Fernández, A.; Viñes, F.; Illas, F. CO_2 Abatement by Two-Dimensional MXene Carbides. *J. Mater. Chem. A* **2018**, 6, 3381-3385.

(28) Morales-Salvador, R.; Morales-García, Á.; Viñes, F.; Illas, F. Two-Dimensional Nitrides as Highly Efficient Potential Candidates for CO_2 Capture and Activation. *Phys. Chem. Chem. Phys.* **2018**, *20*, 17117-17124.

(29) Gouveia, J. D.; Morales-García, Á.; Viñes, F.; Illas, F.; Gomes, J. R. B. MXenes as Promising Catalysts for Water Dissociation. *Appl. Catal. B* **2019**, *260*, 118191 (1-7).

(30) Seh, Z.W.; Fredrickson, K. D.; Anasori, B.; Kibsgaard, J.; Strickler, A.L.; Lukatskaya, M. R.; Gogotsi,Y.; Jaramillo, T.F.; Vojvodic, A. Two-Dimensional Molybdenum Carbide (MXene) as an Efficient Electrocatalyst for Hydrogen Evolution. *ACS Energy Lett.* **2016**, *1*, 589-594.

(31) Yi, S.; Liu, G.; Liu, Z.; Hub, W.; Deng, H. Theoretical Insights into Nitrogen Fixation on Ti_2C and Ti_2CO_2 in a Lithium–Nitrogen Battery. *J. Mater. Chem. A* **2019**, *7*, 19950.

(32) Azofra, L. M.; Li, N.; Douglas, R. M.; Sun, C. Promising Prospects for 2D d^2–d^4 M_3C_2 Transition Metal Carbides (MXenes) in N_2 Capture and Conversion into Ammonia. *Energy Environ. Sci.* **2016**, *9*, 2545.

(33) Ling, C.; Zhang, Y.; Li, Q.; Bai, X.; Shi, L.; Wang, J. New Mechanism for N_2 Reduction: The Essential Role of Surface Hydrogenation. *J. Am. Chem. Soc.* **2019**, *141*, 18264-18270.

(34) Zheng, J.; Liao, F.; Wu, S.; Jones, G.; Chen, T.-Y.; Fellowes, J.; Sudmeier, T.; McPherson, I. J.; Wilkinson, I.; Tsang, S. C. E. Efficient Non-Dissociative Activation of Dinitrogen to Ammonia over Lithium-Promoted Ruthenium Nanoparticles at Low Pressure. *Angew. Chem. Int. Ed.* **2019**, *58*, 2-9.

(35) Cheng, Y.; Dai, J.; Song, Y.; Zhang, Y. Single Molybdenum Atom Anchored on 2D Ti_2NO_2 MXene as a Promising Electrocatalyst for N_2 Fixation. *Nanoscale* **2019**, *11*, 18132-18141.

(36) Gao, Y.; Cao, Y.; Zhuo, H.; Sun, X.; Gu, Y.; Zhuang, G.; Deng, S.; Zhong, X.; Wei, Z.; Li, X.; Wang, J.-G. Mo_2TiC_2 MXene: A Promising Catalyst for Electrocatalytic Ammonia Synthesis. *Catal. Today* **2020**, *339*, 120-126.

(37) Shao, M.; Shao, Y.; Chen, W.; Ao, K. L.; Tong, R.; Zhu, Q.; Chan, I. N.; Ip, W. F.; Shi. X.; Pan, H. Efficient Nitrogen Fixation to Ammonia on MXenes. *Phys. Chem. Chem. Phys.* **2018**, *20*, 14504-14512.

(38) Zhang, J.; Ji, Y.; Wang, P.; Shao, Q.; Li, Y.; Huang, X. Adsorbind and Activating N_2 on Heteregeneous Au-Fe_3O_4 Nanoparticles for N_2 Fixation. *Adv. Func. Mater.* **2019**, 30, 1906579.

(39) Thakur, R.; VahidMohammadi, A.; Moncada, J.; Adams, W. R.; Chi, M.; Tatarchuk, B.; Beidaghi, M.; Carrero, C. A. Insights into the Thermal and Chemical Stability of Multilayered V_2CT_x MXene. *Nanoscale* **2019**, *11*, 10716-10726.

(40) Seredych, M.; Shuck, C. E.; Pinto, D.; Alhabeb, M.; Precetti, E.; Deysher, G.; Anasori, B.; Kurra, N.; Gogotsi, Y. High-Temperature Behavior and Surface Chemistry of Carbide MXenes Studied by Thermal Analysis. *Chem. Mater.* **2019**, *31*, 3324−3332.

(41) Zhang, L.; Su, W.; Huang, Y.; Li, H.; Fu, L.; Song, K.; Huang, X.; Yu, J.; Lin, C. –T. In Situ High-Pressure X-ray Diffraction and Raman Spectroscopy Study of $Ti_3C_2T_x$ MXene. *Nanoscale Res. Lett.* **2018**, *13*, 343.

(42) Yorulmaz, U.; Özden, A.; Perkgöz, N, K.; Ay, F.; Sevik, C. Vibrational and Mechanical Properties of Single Layer MXene Structures: A First-Principle Investigation. *Nanotechnology* **2016**, *27*, 335702.

(43) Kresse, G.; Furthmüller, J. Efficient Iterative Schemes for *Ab Initio* Total-Energy Calculations Using a Plane-Wave Basis Set. *Phys. Rev. B* **1996**, *54*, 11169.

(44) Blöchl, P. E. Projector Augmented-Wave Method. *Phys. Rev. B* **1994**, *50*, 17953-17979.

(45) Monkhorst, H. J.; Pack, J. D. Special Points for Brillouin-Zone Integrations. *Phys. Rev. B.* **1976**, *13*, 5188-5192.

(46) Perdew, J. P.; Burke, K.; Ernzerhof, M. Generalized Gradient Approximation Made Simple. *Phys. Rev. Lett.* **1996**, *77*, 3865-3868.

(47) Grimme, S.; Antony, J.; Ehrlich, S.; Krieg, H. A. Consistent and Accurate *Ab Initio* Parametrization of Density Functional Dispersion Correction (DFT-D) for the 94 Elements H-Pu. *J. Chem. Phys.* **2010**, *132*, 154104.

(48) Evans, M. G.; Polanyi, M. Inertia and Driving Force of Chemical Reactions. *Trans. Faraday Soc.* **1938**, *34*, 11-24.

(49) Brønsted, J. N. Acid and Basic Catalysis. *Chem. Rev.* **1928**, *5*, 231-338.

(50) Bell, R. P. The Theory of Reactions Involving Proton Transfers. *Proc. R. Soc. London Ser. A* 1936, **154**, 414-429.

(51) Naguib, M.; Mochalin, V. N.; Barsoum, M. W.; Gogotsi, Y. 25th anniversary article: MXenes: A New Family of Two-Dimensional Materials. *Adv. Mater.* **2014**, *26*, 992-1005.

(52) Zhu, J.; Ha, E.; Zhao, G.; Zhou, Y.; Huang, D.; Yue, G.; Hub, L.; Sun, N.; Wang, Y.; Yoon, L.; Lee, S.; Xu, C.; Wong, K.-Y.; Astruc, D.; Zhao, P. Recent Advance in MXenes: A Promising 2D Material for Catalysis, Sensor and Chemical Adsorption. *Coord. Chem. Rev.* **2017**, *352*, 306-327.

(53) Morales-García, Á.; Mayans-Llorach, M.; Viñes, F.; Illas, F. Thickness Biased Capture of CO_2 on Carbide MXenes. *Phys. Chem. Chem. Phys.* **2019**, *21*, 23136-23142.

(54) Logadóttir, Á.; Nørskov, J. K. Ammonia Synthesis over a Ru(0001) Surface Studied by Density Functional Calculations. *J. Catal.* **2003**, *220*, 273-279.

(55) Hinrichsen, O.; Rosowski, F.; Muhler, M.; Ertl, G. The Microkinetics of Ammonia Synthesis Catalyzed by Cesium-Promoted Supported Ruthenium. *Chem. Eng. Sci.* **1996**, *51*, 1683-1690.

(56) Klemola, K. T. Chemical Reaction Equilibrium Calculation Task for Chemical Engineering Undergraduates-Simulating Fritz Haber´s Ammonia Synthesis with Thermodynamic Software. *Chem. Eng. Educ.* **2014**, *48*, 115-120.

(57) Prats, H.; Álvarez, L.; Illas, F. Sayós, R. Kinetic Monte Carlo Simulations of the Water Gas Shift reaction on Cu (111) from Density Functional Theory Based Calculations. *J. Catal.* **2016**, *333*, 217-226.

(58) Gokhale, A. A.; Dumesic, A. J.; Mavrikakis, M. On the Mechanism of Low-Temperature Water Gar Shift Reaction on Cooper. *J. Am. Chem. Soc.* **2008**, *130*, 1402-1414.

(59) Filot, I. A. W.; van Santen, R. A.; Hensen, E. J. M. The Optimally Performing Fischer-Tropsch Catalyst. *Angew. Chem., Int. Ed.* **2014**, *53*, 12746-12750.

(60) Filot, I. A. W.; Broos, R. J. P.; van Rijn, J. P. M.; van Heugten, G. J. H.; van Santen, R. A.; Hensen, E. J. M. First-Principles-Based Microkinetics Simulations of Synthesis Gas Conversion on a Stepped Rhodium Surface. *ACS Catal.* **2015**, *5*, 5453-5467.

(61) Casey-Stevens, C. A.; Lambie, S. G.; Ruffman, C.; Skúlason, E.; Garden, A. L. Geometric and electronic Effects Contributting to N_2 Dissociation Barriers on a Range of Active Sites on Ru Nanoparticles. *J. Phys. Chem. C* **2019**, *123*, 30458-30466.

Graphic for TOC